DOI: 10.11835/j.issn.2096-6717.2026.024

开放科学(资源服务)标识码 OSID:

不同MICP处理方法对裂隙岩体抗渗性能的影响试验研究

华海成[1a,1b],王鲁琦[1a,1b,1c,1d],仉文岗[1a,1b,1c,1d],覃长兵[1a,1b],赵彬[2],杨阳[1a]

(1.重庆大学 a.土木工程学院;b.山地城镇建设与新技术重点实验室;c.库区环境地质灾害防治国家地方联合工程研究中心,重庆 400045;d.三峡库区库岸滑坡灾害重庆市野外科学观测研究站,重庆 400045;2.重庆大学建筑规划设计研究总院有限公司,重庆 400045)

摘　要:在长期水位波动作用下,库岸边坡消落带岩体持续损伤劣化,成为现阶段诱发库区岸坡失稳破坏的关键因素。与传统化学注浆加固方法相比,微生物诱导碳酸钙沉积(MICP)技术在改善岩土体强度和抗渗性能的同时,具有低碳环保、对岩土体扰动小的优势,在岩土工程领域具有广泛的应用前景。分别采用MICP注浆沉淀法、活性生物泥法、岩粉注浆法对三峡库区消落带裂隙岩体开展微生物加固试验,并对加固后的裂隙岩体进行CT扫描试验、微观孔隙结构分析,在此基础上开展孔隙尺度的渗流模拟,并结合室内渗透率测试,从多个尺度量化评估不同MICP处理方法对裂隙的填充效果以及对岩体整体抗渗性能的改善效果。结果表明:3种MICP加固技术均能够较好地填充岩体裂隙,有效堵塞裂隙渗流通道,裂隙面孔隙填充率达60%以上,其中岩粉注浆法的孔隙填充效果最好,填充率高达92.6%,并且90.7%的孔隙为孤立孔隙,与常规MICP注浆沉淀方法相比,加固后岩体的渗透率降低了一个数量级。

关键词:微生物诱导碳酸钙沉淀(MICP);裂隙灰岩;消落带基岩;CT扫描;渗流模拟

中图分类号:TU458　　**文献标志码:**A　　**文章编号:**2096-6717(XXXX)XX-0001-16

Experimental study on the influence of MICP treatment methods on the impermeability of fractured rock

HUA Haicheng[1a,1b], *WANG Luqi*[1a,1b,1c,1d], *ZHANG Wengang*[1a,1b,1c,1d], *QIN Changbing*[1a,1b], *ZHAO Bin*[2], *YANG Yang*[1a]

(1a. School of Civil Engineering; 1b. Key Laboratory of New Technology for Construction of Cities in Mountain Area; 1c. National Joint Engineering Research Centre of Geohazards Prevention in the Reservoir Areas; 1d. Chongqing Field Scientific Observation Station for Landslide Hazards in Three Gorges Reservoir Area, Chongqing University, Chongqing 400045, P. R. China; 2. General Research Institute of Architecture & Planning Design Co., Ltd., Chongqing University, Chongqing 400045, P. R. China)

Abstract: Continuous deterioration of reservoir bank rock under periodic water level fluctuations is a key factor triggering slope instability. Unfortunately, this poses significant challenges to the long-term safe operation of hydropower projects in mountainous regions. Conventional rock reinforcement methods are prone to damaging

Received: 2026-01-09

Foundation items: National Natural Science Foundation of China (No. 52308340); China Postdoctoral Foundation (No. 2024M753842)

Author brief: HUA Haicheng (2001-), main research interest: MICP reinforcement methods of fractured rock mass, E-mail: 729403800@qq.com.

ZHANG Wengang (corresponding author), PhD, professor, doctorial supervisor, E-mail: zhangwg@cqu.edu.cn.

the reservoir's ecological environment. Microbial-induced carbonate precipitation (MICP), a widely recognized technology in geotechnical engineering, offers low-carbon, environmentally friendly benefits and minimal disturbance to geomaterials. However, research on the application of MICP to reinforce fractured rock masses in reservoir banks remains relatively scarce. This study focused on rock within the water-level fluctuation zone of the Three Gorges Reservoir Area. Three MICP treatment methods—MICP precipitation, active bio-slurry, and rock powder-amended grouting method (RPGM)—were employed for microbial reinforcement of fractured rock samples. Based on micro-CT scanning and laboratory permeability tests, a multi-scale evaluation method was proposed to quantitatively assess the effectiveness of various MICP methods in improving pore-filling in fractured rock. The results demonstrated that MICP technology effectively reduced the permeability of fractured rock, achieving surface-filling rates exceeding 60%. Notably, the RPGM method yielded the optimal reinforcement effect, achieving a fractured surface filling rate of up to 92.6%, with 90.7% of the pores identified as isolated. Moreover, the permeability of rock reinforced by RPGM was reduced by one order of magnitude compared to the MICP precipitation methods.

Keywords: microbial-induced carbonate precipitation (MICP); fractured limestone; water-level fluctuation zone; X-ray CT scanning; seepage simulation

1 Introduction

During the operation of large-scale hydropower projects in canyon areas, reservoir water levels fluctuate periodically in response to water storage demands[1]. This exposes bank rock masses to continuous, multi-field, coupled damage—including hydraulic fracturing, dissolution-induced deterioration, and stress redistribution—under cyclic wetting-drying conditions[2]. Consequences such as damage accelerate the cracking and degradation of the base rock[3], positioning it as a critical contributing factor in reservoir geo-hazard chains and a universal challenge to the long-term operational safety of hydropower projects[1,4]. Under cyclic wet-dry conditions, water infiltrated through existing cracks in the rock mass, leading to progressive deterioration of the rock's overall physical and mechanical properties[5]. Thus, beyond enhancing mechanical strength, improving impermeability is a critical criterion for evaluating the effectiveness of reinforcement techniques for fractured rock masses in water-level fluctuation zones. Furthermore, the fragile ecological environment of reservoir areas is highly vulnerable to irreversible damage from traditional rock reinforcement techniques (e. g. , chemical grouting, bolt reinforcement), primarily due to their invasive construction processes and the poor environmental compatibility of the materials used.

Microbial-induced Carbonate Precipitation (MICP) is an emerging eco-friendly reinforcement technology that uses the metabolic activity of microorganisms to precipitate various minerals. These precipitates fill and cement the surrounding geomaterials (soil/rock), thereby enhancing their strength and reducing permeability[6]. Moreover, multiple microbial metabolic pathways and enzymatic reactions, such as urea hydrolysis, denitrification, and sulfate reduction, can drive the formation of insoluble inorganic minerals[7-9]. Among these, urea hydrolysis-induced $CaCO_3$ precipitation is considered the most promising and has garnered significant attention in geotechnical engineering[10].

MICP technology was applied to the restoration of soil, stone, and cement-based materials [11-12]. In soil reinforcement, MICP significantly strengthens soil and reduces its porosity and permeability [13-14]. Notably, research on reducing permeability in fractured rock using MICP is relatively scarce[15]. Cuthbert et al. conducted field-scale trials using MICP grouting to seal structural fractures in subsurface rock, thereby validating the feasibility of large-scale MICP application for enhancing the impermeability of engineering structures[16]. Minto et al. also performed MICP grouting on small-scale, artificially fractured rock samples and observed the distribution of $CaCO_3$ crystals within the fractures [17]. Tobler et al. further investigated the influence of different MICP injection strategies on the degree of permeability reduction in fractured granite[18]. These studies

collectively indicate that microbial mineralization products can substantially reduce the permeability of fractured rock and enhance its seepage resistance. Based on the above, MICP technology shows significant potential to reduce the permeability of fractured media. Moreover, carbonate rocks were widely distributed in the Three Gorges Reservoir Area. The mineral composition of these blocks was predominantly calcite, and their chemical composition was mainly calcium carbonate, consistent with the final product of MICP. Therefore, the MICP reinforcement technology offered a new, green approach to repairing fractured rock masses in the Three Gorges Reservoir Area.

Moreover, the relative influence of various factors on the anti-seepage performance of MICP-treated fractured rock remains unclear. Drawing from existing MICP research on soil reinforcement, key influencing factors include the properties of bacterial suspensions and cementation solutions, environmental conditions (e. g. , temperature, pH), and treatment methods[19]. Existing studies on fractured rock primarily focus on bacterial suspension and environmental conditions: Shi et al. investigated the effects of bacteria-to-cementation solution volume ratio, cementation solution concentration, and grouting volume on the impermeability of fractured granite. Their results identified grouting volume as the critical factor, although excessive volume negatively affected permeability reduction[20]. Other researchers have examined the influence of external factors, such as rock fracture surface roughness, distribution of MICP precipitates, fracture aperture, injection pressure, and temperature, on changes in rock mass impermeability [21-23]. Notably, the impact of different MICP treatment methods on rock reinforcement efficacy has received limited systematic investigation. In this paper, a multi-scale evaluation method was proposed to assess the effectiveness of MICP methods for pore-filling in fractures, based on microscopic and laboratory tests.

This research focused on fractured limestone within the water-level fluctuation zone of the Three Gorges Reservoir Area. Three distinct MICP methods commonly used in geomaterial reinforcement-namely, the MICP precipitation method, the active bio-slurry method, and the rock powder-amended microbial grouting method (RPGM) [13,24-25] were employed to reinforce fractured limestone specimens. Post-treatment, X-ray computed tomography (CT) scanning was conducted to reconstruct 3D digital core models of MICP-reinforced limestone, enabling quantitative analysis of pore structure within the fracture-filling cementation. Subsequent pore-scale seepage simulations and gas permeability tests were systematically used to evaluate the multi-scale anti-permeability enhancement of the three MICP methods. The findings aimed to provide practical guidance for applying MICP technology to reinforce fractured rock masses in reservoir banks.

2　Materials and methods

As shown in Fig. 1, during the MICP reaction, urease-producing bacteria utilize environmental urea as both a carbon and a nitrogen source. Through metabolic activity, they generate abundant, highly active urease enzymes[26]. These enzymes subsequently catalyze the hydrolysis of urea in solution, producing carbonate ions (CO_3^{2-}) while concurrently elevating the pH of the local microenvironment. The resulting alkaline conditions facilitate the binding of free calcium ions (Ca^{2+}) to CO_3^{2-}, ultimately inducing the formation of calcium carbonate.

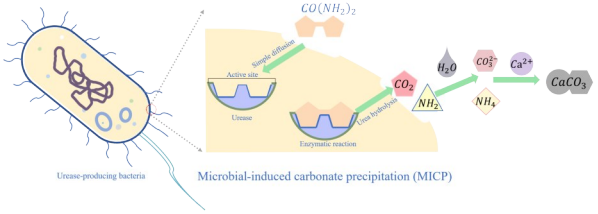

Fig. 1　Schematic diagram of MICP[26]

2.1　Experimental materials preparation

(1) Bacterial suspension and cementation solution

The bacterium *Sporosarcina pasteurii* (strain DSM 33), a ubiquitous and non-pathogenic soil microorganism[27], was employed in this study. The liquid medium used in the cultivation process contained (per liter): 20 g yeast extract, 15 g NH_4Cl, and 0.01 g $NiCl_2$. Following sterilization by autoclaving and UV irradiation, the medium was cooled in a laminar flow hood. Bacterial inoculation was then performed at 1% (v/v) of the medium

volume, followed by incubation in a constant-temperature shaker at 200 r/min for 24 h[28]. The resulting microbial suspension was stored at 4 ℃ before use.

The harvested bacterial suspension was subjected to urease activity and concentration tests to ensure mineralization potential. Urease activity was subsequently evaluated by measuring the change in solution conductivity resulting from urea hydrolysis. Finally, the bacterial concentration was determined by measuring the absorbance (optical density) of the suspension at 600 nm (OD600) using a spectrophotometer. The cultured bacterial suspension exhibited a urease activity greater than 0.1 mS/min and an OD600 value of 1.2±0.5.

The cementation solution required for the test was prepared by dissolving 1.5 mol/L urea and 1.5 mol/L anhydrous $CaCl_2$ in ultrapure water.

(2) Samples preparation

As shown in Fig. 2, limestone was collected from colluvial deposits in the water-level fluctuation zone of bank slopes in the Wushan section of the Three Gorges Reservoir Area. Cylindrical rock specimens (diameter 50 mm, height 100 mm) were drilled from the blocks. To facilitate comparative analysis and minimize variability among samples, each intact specimen was split axially into two halves, and the fractured surfaces were polished to create smooth artificial fractures, resulting in limestone specimens with through-going fractures (Fig. 2(d)).

Note: (a) Wushan section of the Three Gorges Reservoir Area, (b) Fluctuation zone of steep banks, (c) Sampling location, (d) Fractured limestone specimens.

Fig. 2 Preparation procedure of fractured limestone specimens

2.2 MICP treatment methods

2.2.1 MICP precipitation method

The fractured rock specimen was fixed in the mold, with metal strips used to control the fracture apertures, which were maintained at 1 mm. Adopting Whiffin's two-phase grouting strategy[29], the bacterial and cementation solutions were delivered directly into the fracture via two separate injection channels at 1 mL/min, with the bottom drainage outlet sealed (as shown in Fig. 3). An 8-hour static reaction period followed each injection before waste drainage. This cycle was repeated until the fractured surface was filled.

According to existing research[30], a lower pH retards microbially induced cementation, promoting a more uniform distribution of precipitate. The first injection used a bacterial suspension without pH adjustment, which could quickly produce a MICP-cementation reaction between two separate blocks. In subsequent injections, the pH of the bacterial suspension was adjusted to 6.0 until the fracture was progressively filled, resulting in a MICP-reinforced specimen.

2.2.2 Active bio-slurry method

The active bio-slurry method used pre-fabricated bio-slurry with urease activity for reinforcement, eliminating the need for multiple grouting cycles[24]. This technique has been successfully applied to fracture surface repair, with demonstrated effectiveness[31-32]. In this study, this method was introduced to laboratory-scale rock core specimen fracture repair.

Active bio-slurry was prepared as described in previous studies[33]: the bacterial suspension was premixed with 0.4 mol/L $CaCl_2$ and 0.4 mol/L urea, then stirred continuously on a magnetic stirrer for 12 hours to obtain a urease-active microbial bio-slurry. After centrifugation, the supernatant was discarded, and the milky solid phase (retaining urease activity) was collected. This bio-slurry was uniformly applied to fractured surfaces. Reassembled specimens were then immersed in 2 mol/L cementation fluid for 48 h, followed by oven curing.

2.2.3 Rock powder grouting method

Based on the study by Won et al. [34], the addi-

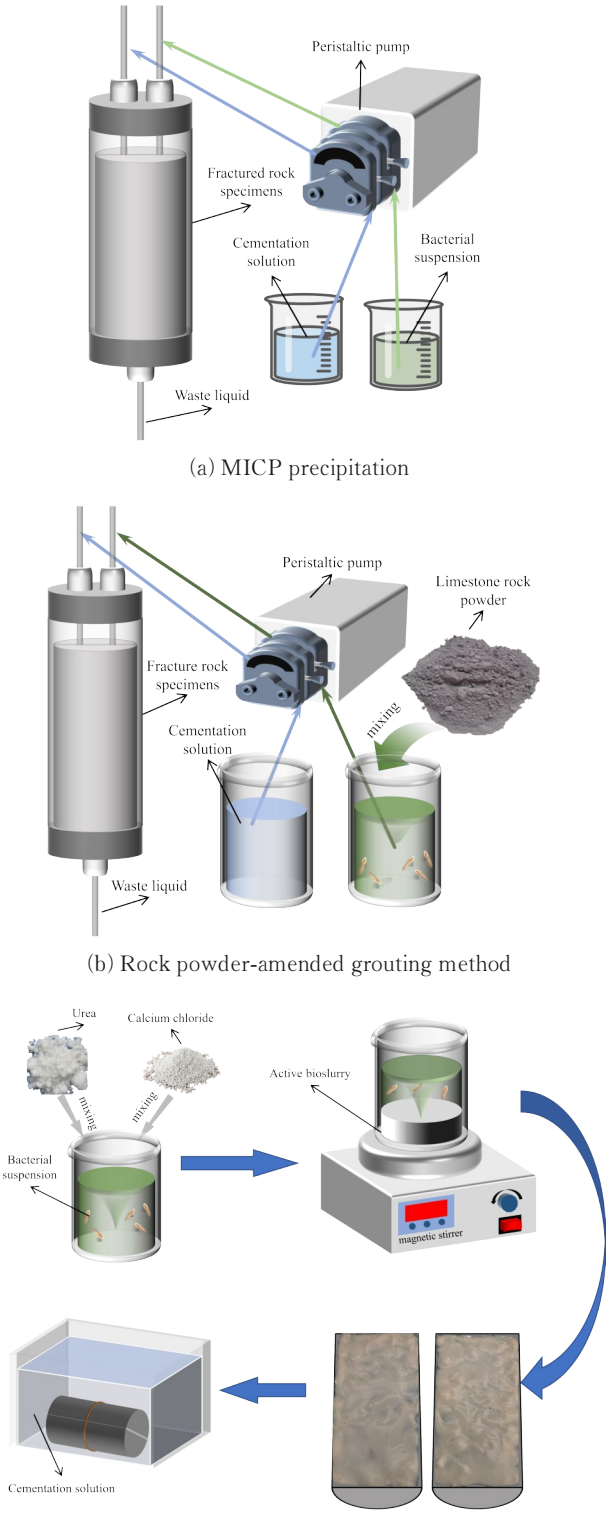

Fig. 3　Flow chart of different MICP processing methods

tion of kaolinite particles to bacterial suspension can promote calcite crystal precipitation, thereby increasing the mass of produced calcium carbonate cement and improving its distribution uniformity. In this study, the aperture of the rock fracture was controlled at approximately 1 mm. Such a relatively large fracture aperture may hinder the formation of calcite crystals. Therefore, to promote heterogeneous nucleation and rapid growth of calcite within the fracture, the collected limestone blocks were ground into a powder (Particle size shown in Fig. 4; D_{50} =16.4 μm) and added to the bacterial suspension. The particle size distribution curve of limestone powder was shown in Fig. 4. The mixture was then stirred evenly using a magnetic stirrer to form a bacterial-limestone powder suspension. The addition of limestone particles provides additional nucleation sites for calcite crystal precipitation. However, excessive fine particles in the bacterial suspension may clog grouting channels, thereby reducing the efficiency of MICP reinforcement[35]. Thus, in this experiment, the concentration of limestone particles in the suspension was controlled below 20 g/L. The other experimental conditions were the same as those used for the MICP precipitation method, and the test was conducted at room temperature.

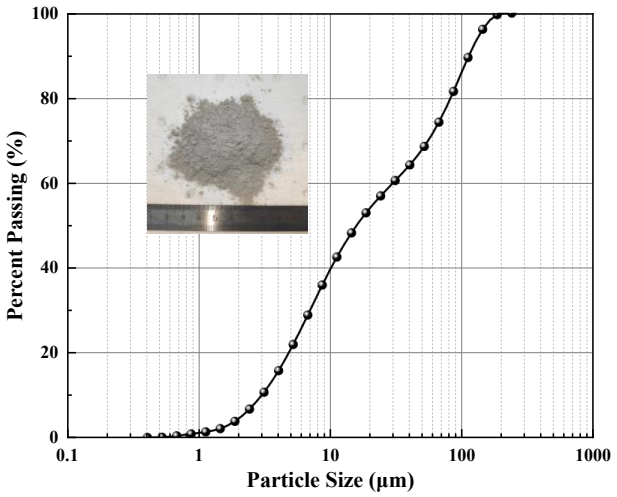

Fig. 4　Particle size distribution curve of limestone powder

2.3　X-ray CT scanning test

X-ray computed tomography (CT) is a non-destructive imaging technique that reconstructs the three-dimensional internal structure of an object by measuring the attenuation of X-rays as they pass through the sample from multiple angular projections, and it has been applied in an increasing number of industries[36]. In microbial geotechnical engineering, micro-CT was used to observe the evolution of calcite formation in pore space and the spatial distribution of mineral phases within rock masses[37].

Specimens treated with different MICP methods underwent X-ray micro-computed tomography at a

voxel resolution of 60.37 μm. The CT scanning equipment used was Phoenix V|tome|x M300 from Waygate Technologies (German). To minimize cone-beam artifacts, specimens were scanned at a 45° inclination, followed by digital realignment. Approximately 1 500 2D grayscale images per specimen were reconstructed in AVIZO software. Median filtering and watershed segmentation were applied to isolate pores and $CaCO_3$ cementation, thereby enabling construction of the digital core of the MICP-reinforced limestone. This digital model enabled quantitative analysis of the internal pore microstructure within fracture-filling cementation and the construction of a 3D pore network model.

2.4 Rock permeability test

Small-scale specimens (diameter 25 mm, height 50 mm) were prepared according to the method in Section 2.1, and microbially treated using the three MICP processing methods in Section 2.2. Helium was employed as the permeating medium due to its chemical inertness, minimal molecular size, low viscosity, and high diffusivity. These properties enabled it to penetrate fine pore channels without reacting with the carbonate rock or the calcium carbonate precipitate, thereby ensuring accurate measurement of porosity and permeability in MICP-reinforced specimens. The test equipment used was the PHI220 porosimeter and CAT112 permeameter (as shown in Fig. 5).

Specimens were oven-dried at 105 ℃ to constant weight before testing. The dried specimen was then sealed in the sample chamber, while the reference chamber was pressurized with high-purity helium to an initial pressure P_1. Upon opening the interconnecting valve, helium expanded into the sample chamber until equilibrium pressure P_2 was attained. According to Boyle's Law, the calculation formula for rock porosity (φ) is as follows:

$$P_1 V_{\text{ref}} = P_2\left(V_{\text{ref}} + V_{\text{matrix}} - V_{\text{grain}}\right) \tag{1}$$

$$V_{\text{grain}} = V_{\text{ref}} + V_{\text{matrix}} - \frac{P_1}{P_2} V_{\text{ref}} \tag{2}$$

$$\varphi = \frac{V_{\text{total}} - V_{\text{grain}}}{V_{\text{total}}} \times 100\% \tag{3}$$

where V_{ref} is the volume of the reference chamber, cm^3; V_{matrix} is the volume of the sample chamber, cm^3; V_{grain} is the grain volume of the rock specimen, cm^3; V_{total} is the whole volume of the rock specimen, cm^3.

The permeability of the core sample was determined using helium. The sample was sleeved with a rubber sleeve and placed in a core mold, where a confining pressure (> 2 MPa) was applied to ensure airtightness between the core and the mold, preventing the test gas from leaking through the gap.

The fluid flow in the rock specimen with a continuous fracture was characterized as single-fracture flow and conformed to the assumption of laminar flow between smooth, parallel plates, as described by the Cubic Law derived from the Navier-Stokes equations[38].

$$Q = -\frac{we^3}{12\mu} \nabla p \tag{4}$$

where Q is the fluid flow rate, m^3/s; w is the fracture width, m; e is the fracture aperture, m; ∇p is the pressure gradient, Pa/m; and μ is the dynamic viscosity of the fluid, Pa•s.

After MICP treatment, the rock fractures were filled with calcium carbonate precipitates, and the cementation body exhibited porous-medium characteristics. Existing studies have demonstrated that filling materials in fractures significantly alter the flow regime and flow paths within fractures. The permeability of filled fractured rock masses is closely related to the properties of the fillings[39]. When fractures are filled, the seepage behavior in fractured rock is no longer characterized by pure, fracture-controlled single fracture flow, and the cubic law ceases to be

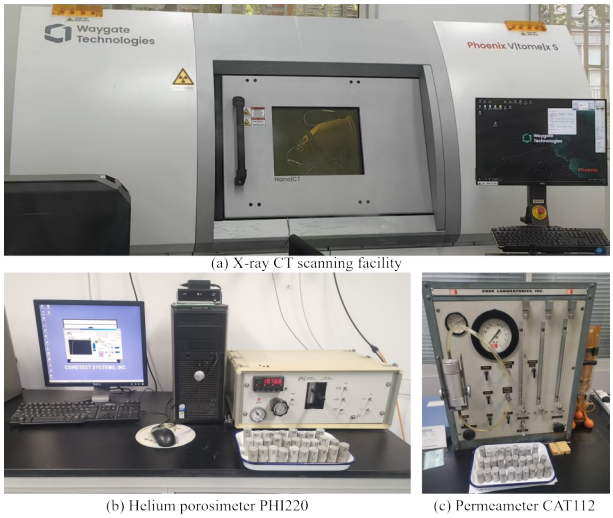

(a) X-ray CT scanning facility

(b) Helium porosimeter PHI220 (c) Permeameter CAT112

Fig. 5 Experimental equipment of CT scanning, porosity, and permeability test

applicable for describing fluid flow within such fractures[40]. The gas permeability of the core sample was calculated using the following formula[41]:

$$k=\frac{2QP_0\mu L}{A\left(P_1^2-P_2^2\right)} \tag{5}$$

where k is the permeability, mD; μ is the dynamic viscosity, Pa·s; L is the length of the sample, cm; Q is the fluid flow rate, cm^3/s; A is the cross-sectional area for fluid flow, cm^2; P_0 is the atmospheric pressure; P_1 is upstream injection gas pressure, MPa; P_2 is downstream outlet pressure, MPa.

3 Results

3.1 Cement condition of fractured surface

The CT data were imported into AVIZO software for alignment correction, and a median filter was applied to remove isolated noise voxels from the CT images. Subsequently, the three-dimensional visualization model of fractured rock specimens was reconstructed.

The CT slice images of the fractured surface in limestone specimens reinforced by three MICP methods were shown in Fig. 6. Following MICP treatment, microbial-induced calcite crystals distributed along fracture planes cemented the separated rock halves into an integrated mass, transforming initially continuous fractures into isolated micropores.

As for the MICP precipitation method, the first-injected bacterial suspension adhered unimpeded to smooth fractured surfaces, rapidly adsorbing calcium ions to form nucleation sites that evolved into cementation bodies. Due to the staged vertical injection scheme (top-down direction with specimen in vertical orientation), calcite precipitation predominantly accumulated at the fracture base distal to the injection port-effectively avoiding clogging issues observed in horizontal injection. However, subsequent injections led to continuous growth and interconnection of precipitates, thereby increasing flow-path tortuosity. The distribution of pore structure within the rock mass changes rapidly, eventually blocking fluid transport. Consequently, while effective cementation occurred at the fracture base, a certain area of cavity appears in the middle and upper areas (black zones in the CT image Fig. 6(d)).

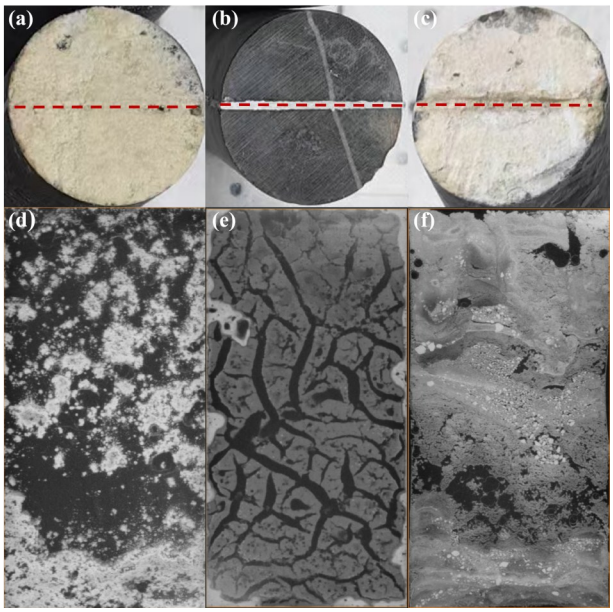

Note: (a) MICP precipitation, (b) Active bio-slurry, (c) RPGM, (d-f) CT scanning images of MICP-reinforced fractures.

Fig. 6　Fractured rock specimens reinforced by MICP and CT scanning images

Bio-slurry with intrinsic urease activity rapidly formed calcite cementation bodies, thereby establishing hydraulic barriers and significantly enhancing short-term impermeability. The active bio-slurry exhibits a certain degree of fluidity, and CT images show that the calcium carbonate cement formed by it is intrusive along the fracture plane and distributed uniformly throughout (Fig. 6(e)). Nevertheless, the low permeability of the limestone matrix impeded the penetration of the cementation solution into the fracture interiors during immersion. Only the outer bio-slurry layer underwent complete mineralization, producing low-permeability crystals. This manifested as: (i) high-CT-value zones (dense $CaCO_3$ precipitation) at fracture boundaries, and (ii) low-CT-value zones (low-density precipitation) in central regions, consistent with the positive correlation between CT gray value and material density.

Injected limestone fines provided nucleation sites where calcite crystals grew radially until bridging the entire fracture aperture (Fig. 6(f)). The generated cement body is relatively uniformly distributed on the fractured surface as a whole, has the best overall filling effect on the fractured surface, and the overall porosity inside the fractured rock mass after reinforcement is the smallest.

3.2 Pore size distribution characteristics

High-density materials appeared bright, while low-density materials appeared dark in CT images. Taking an MICP precipitation-reinforced specimen as an example. The grayscale value distribution of all voxels within the specimen's CT slices is shown in Fig. 7. The overall grayscale distribution exhibited two distinct peaks, corresponding to the internal pores of the rock matrix and the precipitated calcium carbonate cement, respectively. The higher grayscale values represented the limestone matrix itself. A segmentation threshold was set to extract the low-grayscale rock matrix pores.

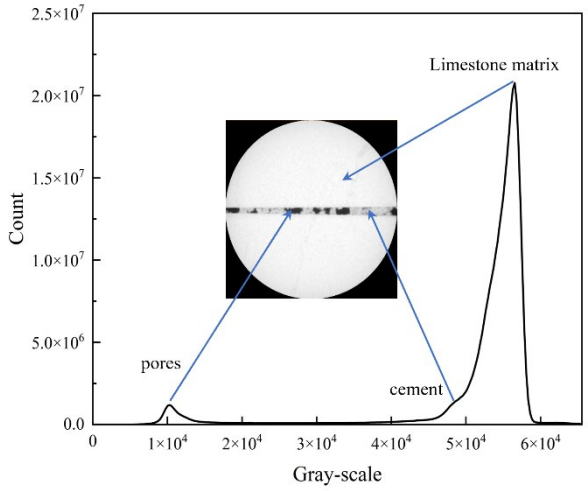

Fig. 7 Grayscale value distribution range of CT images

After CT scanning of the MICP-reinforced specimens, 2D grayscale cross-sectional images were generated along the axial direction at 80 μm intervals, producing over 1200 images per specimen. These images were stacked to reconstruct a 3D digital model of the core specimen. Following segmentation of the pore phase and rock matrix, the "Volume Edit" module was applied to isolate the initial rock fracture region as the study region. The porosity within each 2D slice of the reinforced specimen was then calculated to compare the uniformity of the three MICP reinforcement methods along the axial direction of the fracture (Fig. 8).

For the specimen treated with active bio-slurry, the layer-wise porosity distribution along the axis remained relatively stable, fluctuating between 20% and 40%, indicating a relatively uniform distribution of the calcium carbonate cementation within the rock fracture. In contrast, specimens treated by the two

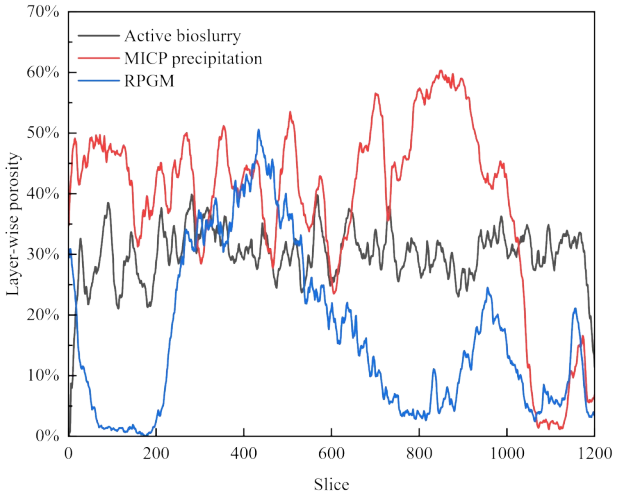

Fig. 8 Layer-wise porosity of specimens reinforced by MICP

injection methods exhibited significant variations in porosity across different layers. Specifically, the sample treated with the MICP precipitation method showed a porosity drop below 5% at the end regions (slices 1050-1150), while porosity in other regions fluctuated considerably, generally remaining above 40%. This suggests that early precipitation at the ends may have blocked subsequent grouting channels. The sample treated with rock powder grouting generally exhibited lower porosity, with 42.48% of the slices having porosity below 10%. Lower porosity was observed at both ends of the specimen, while the middle section showed considerable fluctuation.

Following the import of CT data into AVIZO, a sequential processing workflow was executed. Modules including "Resample Transformed Image," "Volume Edit," and "Median Filter" were employed to correct sample orientation, define the study region, and apply image filtering, respectively, thereby constructing a three-dimensional digital core model. The "Interactive Thresholding" module was subsequently used to segment pores from the rock matrix based on differences in pixel grayscale values. Pore-size information was then extracted and quantitatively analyzed using the "Label Analysis" module. Building on this, the watershed segmentation algorithm[42], which divides regions within images based on intensity and gradient characteristics, was applied to distinguish pore structures from throats and to construct a pore-throat network model. Statistical data of the network elements were ultimately

extracted for quantitative analysis.

Statistical analysis of pore size distribution within the fractured surface of MICP-treated specimens (Table 1, Fig. 9) revealed that the active bio-slurry method significantly increased the proportion of small pores (<500 μm) while reducing large pores (>1 000 μm) compared to the conventional MICP precipitation method. This improvement stems from the more uniform spatial distribution of $CaCO_3$ cementation induced by bio-slurry, resulting in superior fracture filling. Remarkably, the rock powder-amended grouting method (RPGM) exhibited the most substantial reduction in both medium and large pore sizes. This can be attributed to the dual effects of limestone powder: (i) direct physical filling of void spaces, and (ii) accelerated $CaCO_3$ crystallization through abundant nucleation sites, leading to calcium carbonate cement deposited layer by layer in the fracture plane, and large pores were constantly divided into smaller pores.

Based on the extraction of intra-fracture pores, pore network models (PNMs) were constructed by abstracting the pore system into topological networks comprising pores and interconnecting throats. The pore structure represents fluid storage spaces, and the throat represents the potential fluid flow paths between pores.

Statistical analysis of pore-throat information for MICP-treated specimens (Table 2 and Fig. 10) revealed distinct patterns in the distributions of pore-throat size parameters (number of pores/throats, pore size, throat size, throat channel length). Among the three MICP treatment methods, the MICP precipitation method yielded the largest pore-throat parameters. At the same time, those from the RPGM were significantly smaller than those from the active bio-slurry method.

Furthermore, within the generated PNM, the RPGM method identified a significantly higher number of pores than the active bio-slurry method, which in turn identified more pores than the MICP precipitation method. However, the number of throats identified by the RPGM was far lower than that identified by the other two methods. Analysis of pore coordina-

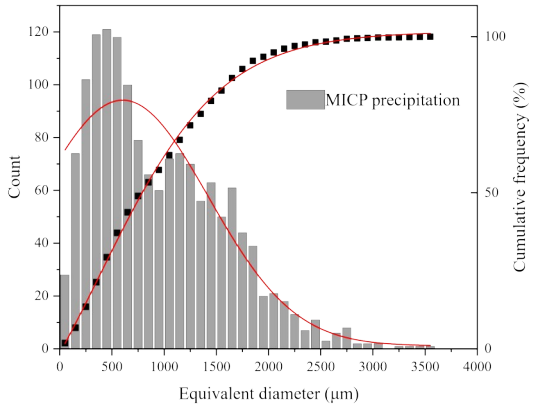

(a) MICP precipitation

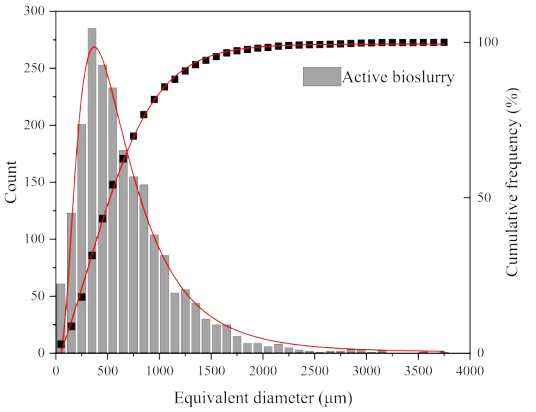

(b) Active bio-slurry

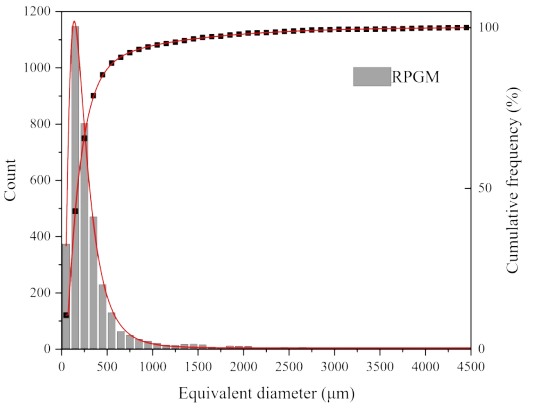

(c) Rock powder-amended grouting

Fig. 9　Histogram of pore size distribution

Table 1　pore size distribution parameter

Pore Eq-diameter/μm	MICP precipitation		Active bio-slurry		RPGM	
	Proportion/%	Volume fraction/%	Proportion/%	Volume fraction/%	Proportion/%	Volume fraction/%
<500	29.35	0.55	43.27	2.05	85.34	2.26
500~1 000	27.96	5.14	38.35	16.96	8.68	4.17
>1 000	42.69	94.30	18.38	80.99	5.98	93.57

Table 2 The number of pores and throats in PNM.

Type	MICP precipitation	Active bio-slurry	RPGM
Pores	1 513	2 133	3 546
Throats	2 728	2 788	321

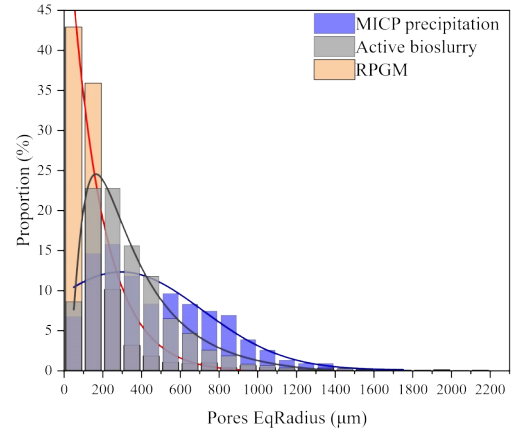

(a) Pores equivalent radius

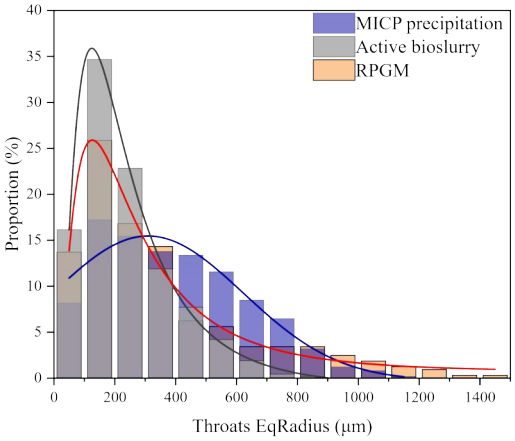

(b) Throats equivalent radius

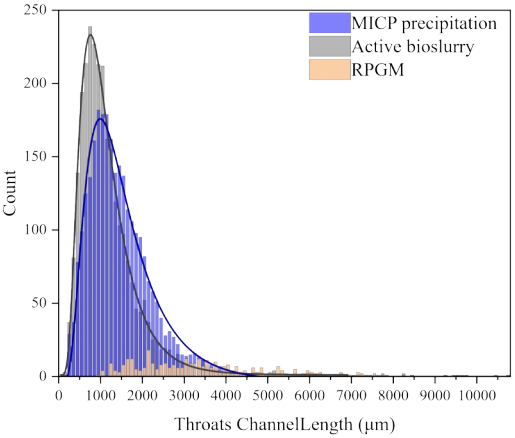

(c) Throats channel length

Fig. 10 Statistical parameters of pore and throat information in PNM

tion numbers revealed that 16.4% of pores in the PNM of the MICP-precipitation specimen had a coordination number of 0, indicating completely isolated pores. This proportion was higher in the active bio-slurry method (22.9%) and dramatically higher in the RPGM (90.7%). This demonstrates that the filling and cementation effects of rock powder particles and microbial precipitates in RPGM-treated specimens transformed the vast majority of pores within the fracture planes from connected pores into isolated pores. Consequently, connected pathways between pores could not be extracted, preventing the formation of effective seepage channels. This mechanism significantly enhances the impermeability of the fractured rock mass.

Notably, sub-voxel pores (smaller than 1 voxel) were undetectable due to the CT resolution limit. Minute pores and flow paths present within the fractured rock mass are not represented in the CT images, potentially leading to an underestimation of true connectivity.

3.3 REV unit analysis

Connectivity assessment confirmed the absence of fully connected pores across fractured surfaces in all MICP-treated specimens. To evaluate the anti-seepage efficacy, a representative elementary volume (REV) was extracted from the digital model center using the Extract Sub-volume module in AVIZO. Porosity was used as the key indicator for determining the REV size. Cubic sub-volumes of varying sizes were extracted from the central region of the fractured rock, and their porosity was calculated. The REV side length was gradually increased until the porosity stabilized as REV size increased and converged to the specimen's global porosity. This stable size was then determined as the final REV dimension. As shown in Fig. 11, when the REV length was increased to 300 voxels, the change in REV porosity tended to stabilize, indicating the optimal REV dimension.

Robust statistical sampling of REVs—achieved by systematically varying their size and location within the digital core—was conducted to ensure analytical reliability amid material heterogeneity and natural variability. This approach confirmed a consistent trend of permeability reduction across all sampled REVs, revealing a uniform response to MICP treatment despite local variations in pore-scale geometry.

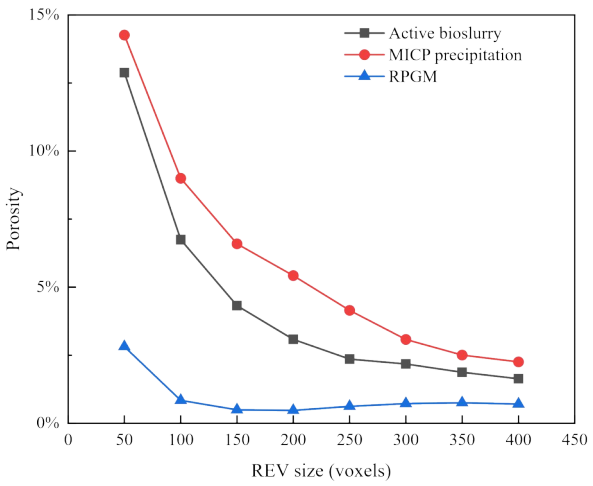

Fig. 11　Porosity of REV units with different sizes

The internal pores, $CaCO_3$ cementation, and limestone matrix in the REV unit were delineated using threshold segmentation of CT data, and pore net models were generated (Fig. 12). The changes in pore-filling rate and the proportion of isolated pores within the REV unit after MICP reinforcement were calculated. Quantitative analysis revealed that the MICP precipitation method increased the pore-filling ratio by 60.09%, with 1.10% of pores isolated. The active bio-slurry method achieved a 63.42% pore-filling enhancement, with 34.11% of pores isolated. Using the rock powder-amended grouting method, 92.63% of pores were filled. Original connected fractures were fragmented into isolated micro-fractures with undetectable flow paths.

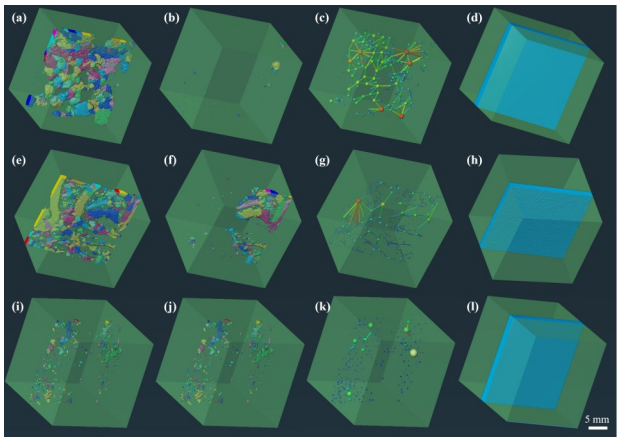

Fig. 12　REV unit pores, isolated pores, PNM, and fractured surface before treatment: REV unit pores, isolated pores, PNM, and fractured surface before treatment

3.4　Pore-scale seepage simulation based on CT images

Based on the pore network model constructed in Section 3.3, the pore network mesh was partitioned in AVIZO, refined in NETFABB (to address self-intersecting elements), and then imported into COMSOL Multiphysics for pore-scale seepage simulation. The Creeping Flow interface was employed for the simulation. Water was defined as a fluid material. After setting the boundary conditions, a pressure gradient of 500 Pa was applied across the inlet-outlet boundary. The generated seepage flow streamlines and pressure gradient distribution were shown in Fig. 13.

For the MICP precipitation method, significant connected pores remained within the fractured surface. A relatively concentrated primary seepage channel was observable across the REV cross-section, and the seepage streamlines were more densely distributed, exhibiting significantly higher seepage velocities internally. Within the bio-slurry-treated REV domain, the streamline was primarily confined to interconnected pores in the left section. Pores located in the upper-right region were isolated and did not contribute to seepage. Consequently, the seepage velocity within the REV was lower than that of the MICP precipitation method. The pore distribution within the RPGM-treated specimen was highly isolated. Crucially, no connected pores were found within a central cubic region measuring 300 voxels along each edge. This indicated the inability to form effective seepage channels through the specimen core.

3.5　Permeability test analysis

Due to specimen size limitations, small-scale fractured rock specimens (diameter 25 mm, height 50 mm) with through-going fractures were prepared. The specimens were reinforced using the MICP treatment methods described in Section 2.2. As shown in Fig. 14, gas permeability was measured under confining pressures of 3, 5, 10, and 15 MPa for all processing conditions.

The results showed that RPGM exhibited the greatest permeability reduction among all MICP treatment methods and significantly improved the permeability resistance of fractured rock, reducing permeability by 1 order of magnitude compared to MICP precipitation method across different confining pressures. It demonstrated that the effective seepage

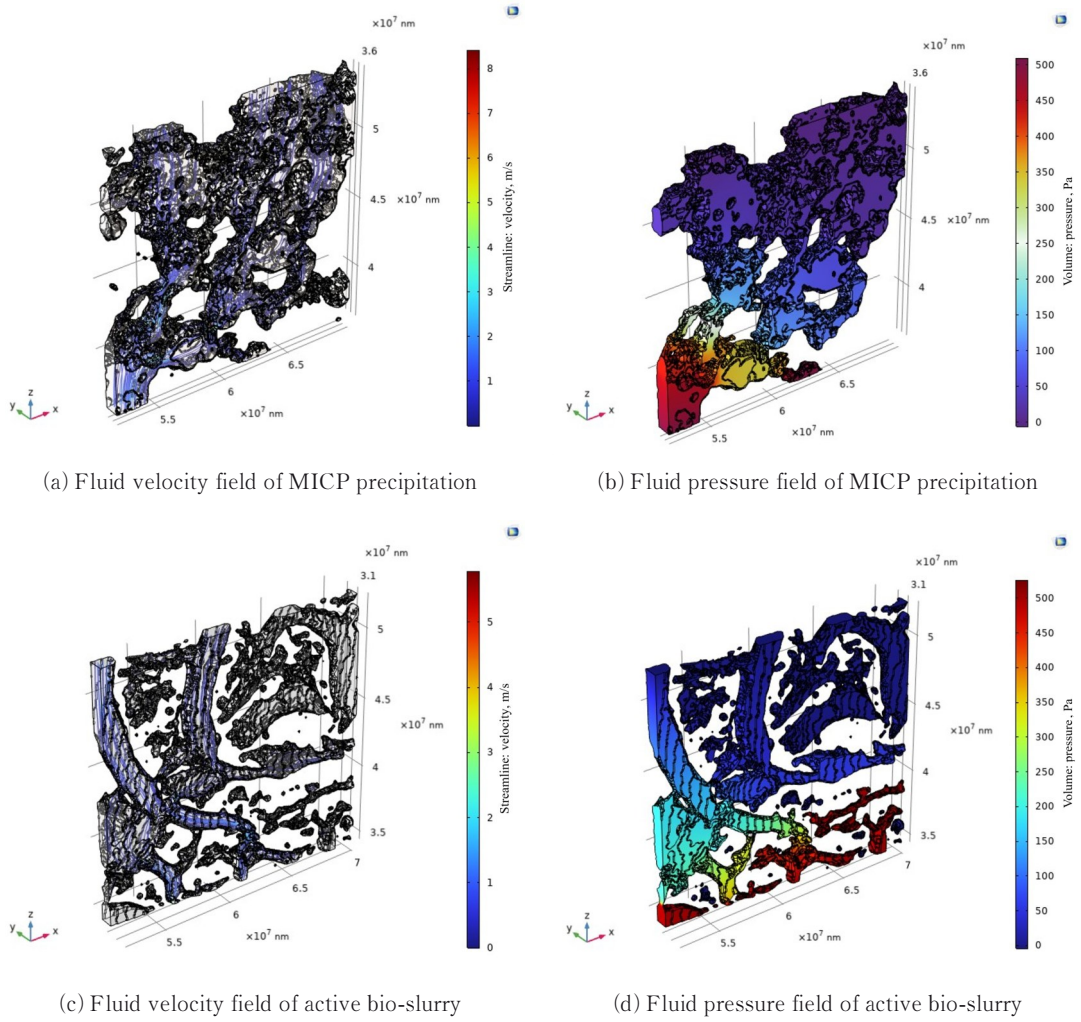

(a) Fluid velocity field of MICP precipitation (b) Fluid pressure field of MICP precipitation

(c) Fluid velocity field of active bio-slurry (d) Fluid pressure field of active bio-slurry

Fig. 13 Absolute seepage simulation: fluid velocity field and fluid pressure field

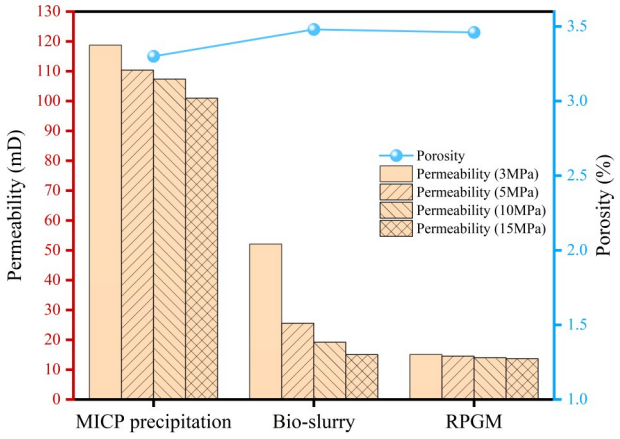

Fig. 14 Porosity and permeability test results of small-scale specimens

path on the fractured surfaces of RPGM-treated specimens was blocked, consistent with previous analysis results for PNM.

Confining pressure exerted a significant influence on gas permeability. The gas permeability of the core samples gradually decreased with increasing confining pressure, at a decelerating rate. The most pronounced reduction occurred within the 3-5 MPa confining-pressure range. Specimens treated with different MICP methods exhibited distinct sensitivities to variations in confining pressure: both the RPGM-reinforced and MICP precipitation-treated specimens maintained relatively stable permeability, whereas the active bio-slurry-treated specimen showed the largest fluctuation in gas permeability, with values substantially higher than those of the other two groups.

Based on CT image analysis, which revealed a low internal density of the fracture-filling precipitate in the bio-slurry specimen, the pore structures within the calcium carbonate precipitate were likely damaged by confining pressure and gas-flow scouring. This process, which reconnected isolated pores, formed new seepage pathways. When subjected to higher confining pressure, the cementation became more compact, thereby reducing the aperture of seepage channels and gradually stabilizing permeability.

Analysis based on CT images suggested that the low internal density of the fracture-filling cement in the bio-slurry specimen may have led to the destruction of pore structures within the calcium carbonate precipitate under the combined effect of confining pressure and gas-flow erosion. This could have reconnected isolated pores and formed new seepage pathways. Under high confining pressure, the cementation was compacted, reducing the aperture of seepage channels, and Gas permeability tended to stabilize gradually.

MICP-reinforced specimens exhibited similar porosity, and the pore structure within the fracture infill remained the dominant pathway for fluid flow. However, distinct differences in pore spatial distribution and connectivity characteristics resulted in markedly differentiated actual permeability. Diameter measurements taken after the gas permeability tests revealed a slight reduction relative to the pre-test dimensions, suggesting that a small number of weak cementations within the fracture may have been compressed or partially crushed under high confining pressure. The resulting fragments could block seepage channels, thereby contributing to the observed reduction in permeability.

4 Discussion

Quantitative analysis of internal pore structures is commonly applied to typical porous materials such as tight sandstones and carbonate matrices[43-45]. Some researchers also applied this methodology to fractured porous rocks with complex micro-fracture networks [46-47]. In this study, the research object was MICP-reinforced fractured rock. CT scan images revealed that after MICP treatment, no fully interconnected fractures remained within the rock fracture surface. Instead, the infilled region exhibited characteristics of a porous medium. Existing studies indicate that the permeability of filled fractured rock is closely related to the porosity and structural distribution of the infill material[48-49]. Therefore, quantitative analysis of the pore structure of the fracture-filling material contributes to a better understanding, analysis, and simulation of fluid flow within the fracture plane, ultimately helping to explain the observed macroscopic permeability variations. Notably, in CT data analysis, due to scanning-resolution constraints, pores smaller than the system′s resolution threshold remained undetectable. Consequently, sub-resolution micropores within the rock were not captured in the dataset, leading to a systematic overestimation of the calculated pore-filling rates. This limitation introduced quantifiable discrepancies between CT-based seepage simulation and experimentally measured permeability values in fractured limestone.

Previous studies on MICP-based remediation of hydraulic properties in fractured rock predominantly employed the two-phase grouting method[17,50-51], demonstrating that MICP grouting can achieve a fracture-filling rate of 67% in granite. This thereby reduces permeability by three orders of magnitude. The calcium carbonate filling rate aligned with the results obtained using the MICP precipitation method in this study. This study introduced the active bio-slurry method for laboratory-scale repair of fractured limestone specimens and compared its performance with conventional grouting. This method enabled rapid sealing of rock fractures without repeated injections, significantly improving efficiency and ensuring a more uniform precipitate. However, the infilled precipitate exhibited low density, making it prone to scouring and potential secondary seepage. At the same time, this laboratory-scale study demonstrated feasibility. Thus, further optimization of application methodology is necessary to facilitate its practical implementation in the field. Moreover, when fracture apertures exceed a critical threshold, traditional MICP grouting fails[52]. To investigate this further, this study comparatively evaluated rock powder-amended grouting—applicable for large-aperture fractures—against other MICP methods. Results demonstrated that limestone powder injection significantly enhances the fracture filling rate (up to 92.6%), effectively altering the connectivity characteristics of pore networks within fractured surfaces and thereby drastically reducing seepage capacity.

Beyond anti-seepage performance, the study indicated that MICP technology can significantly improve the mechanical strength of fractured sandstone and granite[53]. Nevertheless, current research achievements in MICP reinforcement have remained predominantly confined to laboratory-scale specimen

testing, with no large-scale model tests applicable to engineering practice. As such, this study validated the feasibility of MICP for improving the anti-seepage capacity of fractured limestone. Combined with numerical simulation, quantitative analysis of the distribution of the internal micro-pore structure and potential seepage pathways was conducted to elucidate the underlying reasons for the reduction of macroscopic permeability. The enhancement of mechanical strength in MICP-reinforced fractured limestone specimens will be systematically investigated in subsequent research.

5 Conclusion

This study investigated three MICP treatment methods (MICP precipitation, active bio-slurry, and rock powder-amended grouting) to reinforce fractured limestone in the water-level fluctuation zone of the Three Gorges Reservoir Area. X-ray CT scanning, seepage simulation, and permeability tests were conducted to reveal distinct improvements in pore structure and anti-seepage performance. The following results were drawn:

(1) Three MICP reinforcement methods generated calcium carbonate precipitation on fractured rock surfaces, cementing fractures, and filling internal pores. Specifically, the pore-filling rates within the fractured surface achieved by MICP precipitation, active bio-slurry, and the rock powder-amended grouting method were 60.09%, 63.42%, and 92.63%, respectively.

(2) The calcium carbonate precipitation generated by MICP significantly altered the spatial distribution characteristics and connectivity architecture of pores within fractured surfaces. X-ray CT analysis demonstrated that RPGM achieved the most substantial reinforcement: 42.5% of slices exhibited 2D areal porosity below 10%; over 90% of internal pores were isolated; REV analysis showed that no connected pores were detected.

(3) The change in internal pore connectivity structures contributed significantly to the reduced permeability of fractured limestone. Thus, three MICP methods effectively enhanced the anti-seepage capacity of fractured limestone, with RPGM achieving the greatest impermeability enhancement, resulting in a permeability 1 order of magnitude lower than MICP precipitation method.

References

[1] Tang H M, Wasowski J, Juang C H. Geohazards in the three Gorges Reservoir Area, China: lessons learned from decades of research [J]. Engineering Geology, 2019, 261: 105267.

[2] Wang X G, Wang J D, Gu T F, et al. A modified Hoek-Brown failure criterion considering the damage to reservoir bank slope rocks under water saturation-dehydration circulation [J]. Journal of Mountain Science, 2017, 14 (4): 771-781.

[3] Wang L Q, Yin Y P, Zhou C Y, et al. Damage evolution of hydraulically coupled Jianchuandong dangerous rock mass [J]. Landslides, 2020, 17(5): 1083-1090.

[4] Deng H F, Zhang Y C, Zhi Y Y, et al. Sandstone dynamical characteristics influenced by water-rock interaction of bank slope [J]. Advances in Civil Engineering, 2019, 2019: 3279586.

[5] Wang X G, Lian B Q, Wang J D, et al. Creep damage properties of sandstone under dry-wet cycles [J]. Journal of Mountain Science, 2020, 17(12): 3112-3122.

[6] Yang Y, Chu J, Cao B, et al. Biocementation of soil using non-sterile enriched urease-producing bacteria from activated sludge [J]. Journal of Cleaner Production, 2020, 262: 121315.

[7] Qabany AAL, Soga K. Effect of chemical treatment used in MICP on engineering properties of cemented soils [J]. Géotechnique, 2013, 63(4): 331-339.

[8] Warthmann R, van Lith Y, Vasconcelos C, et al. Bacterially induced dolomite precipitation in anoxic culture experiments [J]. Geology, 2000, 28(12): 1091-1094.

[9] van Paassen L A, Ghose R, van der Linden T J M, et al. Quantifying biomediated ground improvement by ureolysis: large-scale biogrout experiment [J]. Journal of Geotechnical and Geoenvironmental Engineering, 2010, 136(12): 1721-1728.

[10] El Mountassir G, Minto J M, van Paassen L A, et al. Applications of microbial processes in geotechnical engineering[M]//Advances in Applied Microbiology. Amsterdam: Elsevier2018: 39-91.

[11] Mu B G, Gui Z Y, Lu F, et al. Microbial-induced carbonate precipitation improves physical and structural properties of Nanjing ancient city walls [J]. Materials, 2021, 14(19): 5665.

[12] Liu S Y, Yu J, Peng X Q, et al. Preliminary study on repairing tabia cracks by using microbially induced carbonate precipitation [J]. Construction and Building

Materials, 2020, 248: 118611.

[13] Chu J, Ivanov V, Naeimi M, et al. Optimization of calcium-based bioclogging and biocementation of sand [J]. Acta Geotechnica, 2014, 9(2): 277-285.

[14] Liu J, Li G, Li X A. Geotechnical engineering properties of soils solidified by microbially induced $CaCO_3$ precipitation (MICP) [J]. Advances in Civil Engineering, 2021, 2021: 6683930.

[15] Wu C Z, Chu J, Wu S F, et al. Quantifying the permeability reduction of biogrouted rock fracture [J]. Rock Mechanics and Rock Engineering, 2019, 52(3): 947-954.

[16] Cuthbert M O, McMillan L A, Handley-Sidhu S, et al. A field and modeling study of fractured rock permeability reduction using microbially induced calcite precipitation [J]. Environmental Science & Technology, 2013, 47 (23): 13637-13643.

[17] Minto J M, MacLachlan E, El Mountassir G, et al. Rock fracture grouting with microbially induced carbonate precipitation [J]. Water Resources Research, 2016, 52(11): 8827-8844.

[18] Tobler D J, Minto J M, El Mountassir G, et al. Microscale analysis of fractured rock sealed with microbially induced $CaCO_3$ precipitation: influence on hydraulic and mechanical performance [J]. Water Resources Research, 2018, 54(10): 8295-8308.

[19] Tang C S, Yin L Y, Jiang N J, et al. Factors affecting the performance of microbial-induced carbonate precipitation (MICP) treated soil: a review [J]. Environmental Earth Sciences, 2020, 79(5): 94.

[20] Shi L, Yang X, Li J X, et al. Investigation on the influence factor for the permeability reduction effect in biogrouted fracture using stage injection strategy [J]. Engineering Geology, 2025, 345: 107869.

[21] Ai G Z, Wu C Z, Zhang S X, et al. Temporal-spatial evolution of MICP precipitates in biogourted rock fracture with different roughness [J]. Tunnelling and Underground Space Technology, 2025, 157: 106327.

[22] De Muynck W, Verbeken K, De Belie N, et al. Influence of temperature on the effectiveness of a biogenic carbonate surface treatment for limestone conservation [J]. Applied Microbiology and Biotechnology, 2013, 97(3): 1335-1347.

[23] Peng S Q, Zhang K J, Fan L, et al. Permeability reduction and electrochemical impedance of fractured rock grouted by microbial-induced calcite precipitation [J]. Geofluids, 2020, 2020: 8876400.

[24] Cheng L, Shahin M A. Urease active bioslurry: a novel soil improvement approach based on microbially induced carbonate precipitation [J]. Canadian Geotechnical Journal, 2016, 53(9): 1376-1385.

[25] GAO R, LUO Y, DENG H. Experimental study on repair of fractured rock mass by microbial induction technology [J]. R Soc Open Sci, 2019, 6(11): 191318.

[26] Zhang J H, Shi X Z, Chen X, et al. Microbial-induced carbonate precipitation: a review on influencing factors and applications [J]. Advances in Civil Engineering, 2021, 2021: 9974027.

[27] KHOSHTINAT S. Advancements in Exploiting Sporosarcina pasteurii as Sustainable Construction Material: A Review[J]. Sustainability, 2023, 15(18)

[28] Yang Y, Han S K, Liu H L, et al. Influence of particle size distribution on biocarbonation method produced microbial restoration mortar for conservation of sandstone cultural relics [J]. Biogeotechnics, 2023, 1(4): 100051.

[29] Whiffin V S, van Paassen L A, Harkes M P. Microbial carbonate precipitation as a soil improvement technique [J]. Geomicrobiology Journal, 2007, 24(5): 417-423.

[30] Cheng L, Shahin M A, Chu J. Soil bio-cementation using a new one-phase low-pH injection method [J]. Acta Geotechnica, 2019, 14(3): 615-626.

[31] Yang Y, Zhang C, He X, et al. Feasibility study on repairing simulated heritage bricks using bioslurry induced calcium carbonate [J]. Rock and Soil Mechanics, 2025, 46(6): 1777-1787.

[32] Yu X N, Zhang Z H. Calcium carbide sludge activated fly ash mixture for offshore construction and its crack repair using seawater-mixed bioslurry cement [J]. Journal of Cleaner Production, 2023, 395: 136456.

[33] Yang Y, Chu J, Xiao Y, et al. Seepage control in sand using bioslurry [J]. Construction and Building Materials, 2019, 212: 342-349.

[34] Won J, Jeong B, Lee J, et al. Facilitation of microbially induced calcite precipitation with kaolinite nucleation [J]. Géotechnique, 2021, 71(8): 728-734.

[35] Ma G L, He X, Jiang X, et al. Strength and permeability of bentonite-assisted biocemented coarse sand [J]. Canadian Geotechnical Journal, 2021, 58(7): 969-981.

[36] Wu Y Q, Tahmasebi P, Lin C Y, et al. A comprehensive study on geometric, topological and fractal characterizations of pore systems in low-permeability reservoirs based on SEM, MICP, NMR, and X-ray CT experiments [J]. Marine and Petroleum Geology, 2019, 103: 12-28.

[37] Yang E, Baek S, Kwon T H, et al. X-ray CT-based interpretation of microbial-induced carbonate precipitation and local hydraulic behaviors [J]. Engineering Geology, 2024, 330: 107426.

[38] Witherspoon P A, Wang J S Y, Iwai K, et al. Validity of Cubic Law for fluid flow in a deformable rock fracture [J]. Water Resources Research, 1980, 16(6): 1016-1024.

[39] Sui Q, Yang D S, Chen W Z, et al. Experimental investigation on the transmissivity of fractured granite filled with different materials [J]. Bulletin of Engineering Geology and the Environment, 2022, 81: 1.

[40] Liu R C, Jing H W, He L X, et al. An experimental study of the effect of fillings on hydraulic properties of single fractures [J]. Environmental Earth Sciences, 2017, 76(20): 684.

[41] Zhang H, Zhang J, Du S L, et al. Permeability characteristics of filled fractured coal-rock mass under stress-seepage coupling [J]. Rock Mechanics and Rock Engineering, 2025, 58(11): 11899-11920.

[42] Yuan H Z, Zhang Z X, Huang X, et al. Comparing, slurry infiltration characteristics between calcareous and silica sands based on slurry infiltration column tests and CT scanning [J]. Tunnelling and Underground Space Technology, 2024, 152: 105919.

[43] Ishola O, Vilcáez J. Augmenting X-ray micro-CT data with MICP data for high resolution pore-scale simulations of flow properties of carbonate rocks [J]. Geoenergy Science and Engineering, 2024, 239: 212982.

[44] Li Y, Chi Y M, Han S L, et al. Pore-throat structure characterization of carbon fiber reinforced resin matrix composites: employing Micro-CT and Avizo technique [J]. PLoS One, 2021, 16(9): e0257640.

[45] Rabbani A, Ayatollahi S, Kharrat R, et al. Estimation of 3-D pore network coordination number of rocks from watershed segmentation of a single 2-D image [J]. Advances in Water Resources, 2016, 94: 264-277.

[46] Jing D J, Meng X X, Ge S C, et al. Reconstruction and seepage simulation of a coal pore-fracture network based on CT technology [J]. PLoS One, 2021, 16(6): e0252277.

[47] Watanabe N, Ishibashi T, Hirano N, et al. Precise 3D numerical modeling of fracture flow coupled with X-ray computed tomography for reservoir core samples [J]. SPE Journal, 2011, 16(3): 683-691.

[48] Yue L, Li W, Liu Y, et al. A review of mechanical deformation and seepage mechanism of rock with filled joints [J]. Deep Underground Science and Engineering, 2024, 3(4): 439-466.

[49] Zhao N, Wang Y C, Meng B, et al. Numerical simulation on the seepage properties of soil-rock mixture [J]. Advances in Materials Science and Engineering, 2018, 2018: 1859319.

[50] CHENG L, XIAO Y, DENG H F, et al. Isolation and culture of a native urease-producing bacterium and its application in the reinforcement of fractured rock mass [J]. Rock and Soil Mechanics, 2022, 43(Sup2): 307-314.

[51] Wu C Z, Chu J, Wu S F, et al. 3D characterization of microbially induced carbonate precipitation in rock fracture and the resulted permeability reduction [J]. Engineering Geology, 2019, 249: 23-30.

[52] Song Z C, Wu C Z, Li Z Y, et al. Fracture sealing based on microbially induced carbonate precipitation and its engineering applications: a review [J]. Biogeotechnics, 2024, 2(4): 100100.

[53] Deng J R, Deng H W, Zhang Y N, et al. Experimental study on microbial-induced calcium carbonate precipitation repairing fractured rock under different temperatures [J]. Sustainability, 2022, 14(18): 11770.

(编辑 XXX)